

# Orbital susceptibility of T-graphene: Interplay of high-order van Hove singularities and Dirac cones

D. O. Oriekhov,<sup>1</sup> V. P. Gusynin,<sup>2</sup> and V. M. Loktev<sup>2,3</sup>

<sup>1</sup>*Instituut-Lorentz, Universiteit Leiden, P.O. Box 9506, 2300 RA Leiden, The Netherlands*

<sup>2</sup>*Bogolyubov Institute for Theoretical Physics, National Academy of Science of Ukraine,  
14-b Metrologichna Street, Kyiv, 03680, Ukraine*

<sup>3</sup>*National Technical University of Ukraine KPI, 37 Peremogy Ave., Kyiv, 03056, Ukraine*  
(Dated: September 15, 2020)

Square-octagon lattice underlies the description of a family of two-dimensional materials such as tetragraphene. In the present paper we show that the tight-binding model of square-octagon lattice contains both conventional and high-order van Hove points. In particular, the spectrum of the model contains flat lines along some directions composed of high-order saddle points. Their role is analyzed by calculating orbital susceptibility of electrons. We find that the presence of van Hove singularities of different kinds in the density of states leads to strong responses: paramagnetic for ordinary singularities and more complicated for high-order singularities. It is shown that the orbital susceptibility as a function of hoppings ratio reveals the dia- paramagnetic phase transition. The results for the tight-binding model are compared with low-energy effective pseudospin-1 model near the three band touching point.

## I. INTRODUCTION

The square-octagon lattice attracted attention in connection with graphene allotropes such as planar (tetragraphene) and buckled T-graphenes, both demonstrated using Density Functional Theory (DFT) in Ref.[1]. Several previous attempts to find such allotropes were made in Refs.[2 and 3]. It was noted that planar T-graphene allotrope should be the most stable one after graphene while the buckled T-graphene is not stable, rather it is very similar to planar T-graphene [4]. Recently, the tetragraphene allotrope has been predicted to possess superconductivity with critical temperature up to 20.8 K [5].

Some analytical properties of tight-binding model for T-graphene were studied in Ref.[6], the phase diagrams were analyzed and the existence of Mott metal-insulator phase transitions in the Hubbard model on square-octagon lattice was pointed out [7–11]. In addition, the DFT calculation was already performed in Refs.[12–15] and the kinetic stability with time was analyzed in Ref.[16]. In recent paper [17] the stability of multilayer materials such as ZnO composed of square-octagon lattice was studied with the help of DFT technique. Also it was shown that MoS<sub>2</sub> transition metal dichalcogenide with square-octagon lattice can possess Dirac fermions with Fermi velocity comparable to that of graphene [9]. The coexistence of Dirac fermions and nearly flat bands in this lattice motivates us to study physical quantities such as orbital susceptibility in terms on newly introduced concept of high-order van Hove singularities (VHS) [18].

As is known, when the doping level approaches VHS, system can exhibit strong responses such as orbital paramagnetism in two-dimensional case [19] or chiral superconductivity in the case of graphene [20]. An *ordinary* VHS in two-dimensional electron system corresponds to

logarithmic divergence of the density of states (DOS). The distinctive feature of high-order VHS is a more singular, power-law divergence of DOS with an asymmetric peak [18 and 21]. At the same time, the recent studies of two-dimensional lattices uncovered a wide family of exotic band structures [22] with flat bands and multi-band touching points, at which the quasiparticles are effectively described by high-pseudospin Hamiltonians. Flat bands can be analyzed as a limiting case of VHS with delta-function divergence of DOS. The prominent examples of materials with high-order VHS of different kind are bilayer graphene with tuned dispersion with the help of an interlayer voltage bias [23], Sr<sub>3</sub>Ru<sub>2</sub>O<sub>7</sub> [24] and  $\beta$ -YbAlB<sub>4</sub> [25]. Recently it was also shown, that when a high-order VHS is placed close to the Fermi level, density wave and Pomeranchuk orders, and superconductivity can all be enhanced [26]. The role of high-order VHS on different pairing types in twisted bilayer graphene was analyzed in Ref.[27].

The orbital susceptibility [28] measures the response of a time reversal invariant electronic system to an external magnetic field. Below we use the formulas for susceptibility derived in Refs.[29] and [30] to evaluate susceptibility of T-graphene analytically and numerically. We analyze the role of VHS of both kinds in orbital susceptibility for electrons on square-octagon lattice. Particularly, we show that the flat lines in tight-binding band structure, which were firstly mentioned in Ref.[8], also represent high-order VHS with inverse square root divergence of DOS.

The paper is organized as follows. In Sec.II we describe the tight-binding Hamiltonian of square-octagon lattice. Then, in Sec.III we identify the effective theory that describe bands around highly-symmetric points in Brillouin zone (BZ). Also we identify the type of VHS which are present in T-graphene. In Sec.IV we perform numerical evaluation of susceptibility, and then analyze the qualitative physical effects of Dirac cones (Sec.IV B) and VHS

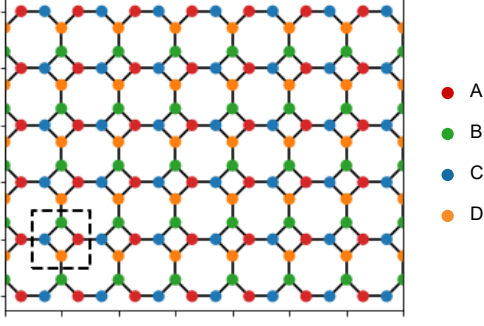


FIG. 1. T-graphene lattice structure, which is described in main text. Each sublattice is denoted by its own color. Black dashed rectangle encircles one elementary cell.

using effective low-energy expansion. The role of high-order VHS is discussed also in the Conclusions (Sec.V) where we summarize the obtained results. In Appendix B we give expression for the Green function of T-graphene.

## II. TIGHT-BINDING MODEL

The square-octagon lattice consists of four atoms per unit cell which form a small square, and is shown on Fig.1. According to Ref. [3], the numerical values are equal for nearest neighbor interatomic distances  $d = 1.429\text{\AA}$  (which are all approximately equal) and lattice constant  $a = 3.47\text{\AA}$  for T-graphene. Ref.[6] gives the intra-square,  $1.48\text{\AA}$ , and inter-squares,  $1.35\text{\AA}$ , distances, and similar values were reported in Ref.[17]. The basis vectors of Bravais lattice and reciprocal lattice are

$$\begin{aligned} \mathbf{a}_1 &= (a, 0), \quad \mathbf{a}_2 = (0, a); \\ \mathbf{b}_1 &= \left(0, \frac{2\pi}{a}\right), \quad \mathbf{b}_2 = \left(\frac{2\pi}{a}, 0\right). \end{aligned} \quad (1)$$

In the tight-binding model, we take hopping parameters between atoms in two neighboring small squares to be  $t_1$ , and inside small square  $t_2$ . The corresponding tight-binding Hamiltonian has the form [6 and 8]

$$H_{Tg}(\mathbf{k}) = - \begin{pmatrix} 0 & t_2 & t_1 e^{ik_x a} & t_2 \\ t_2 & 0 & t_2 & t_1 e^{ik_y a} \\ t_1 e^{-ik_x a} & t_2 & 0 & t_2 \\ t_2 & t_1 e^{-ik_y a} & t_2 & 0 \end{pmatrix}. \quad (2)$$

The above mentioned difference in interatomic distances can effectively be described by tuning the hopping parameters  $t_1$  and  $t_2$ . The values of these hopping parameters can be taken from DFT calculations:  $t_1 = 2.9\text{ eV}$  and  $t_2 = 2.5\text{ eV}$  were used in Ref.[6], while  $t_1 = 2.98\text{ eV}$  and  $t_2 = 2.68\text{ eV}$  were found from DFT calculations inside one layer of octagraphene [31].

The spectrum can be found from the equation  $\det[\varepsilon\mathbb{I} - H_{Tg}(\mathbf{k})] = 0$ , which after simplification reduces to [6 and 8]

$$\begin{aligned} \varepsilon^4 - 2(t_1^2 + 2t_2^2)\varepsilon^2 + 4t_1t_2^2(\cos(ak_x) + \cos(ak_y)) - \\ - 4t_1^2t_2^2\cos(ak_x)\cos(ak_y) + t_1^4 = 0, \end{aligned} \quad (3)$$

and has the form of depressed quartic equation. The spectrum is symmetric with respect to rotations on the angle  $\frac{\pi}{4}$  in  $k$ -space, because the lattice has a  $C_4$  point symmetry group. Also the spectrum is symmetric with respect to transformations  $\varepsilon \rightarrow -\varepsilon$  together with  $k_x \rightarrow k_x \pm \frac{\pi}{a}$ ,  $k_y \rightarrow k_y \pm \frac{\pi}{a}$  (called chiral symmetry in [8]). The Brillouin zone of square-octagon lattice is a square with  $-\frac{\pi}{a} < k_x, k_y < \frac{\pi}{a}$ . The corresponding highly-symmetric points are defined as

$$\begin{aligned} \Gamma &= (0, 0), \quad M = \left(\pm\frac{\pi}{a}, \pm\frac{\pi}{a}\right), \\ X &= \left(\pm\frac{\pi}{a}, 0\right), \quad \left(0, \pm\frac{\pi}{a}\right), \end{aligned} \quad (4)$$

and are located in the center, corners and the middle of each square site, respectively. It is convenient to measure the energy in terms of  $t_1$  hopping parameter, and introduce the dimensionless relation between hopping parameters  $\alpha = t_2/t_1$ . The 3D plots of spectrum defined by Eq.(3) for several values of  $\alpha$  are shown in Fig.2, while the 2D plots along highly-symmetric lines are represented in Fig.3. For  $\alpha = 1$ , near the three band touching points  $\Gamma$  and  $M$ , one observes almost flat middle bands [8]. These two middle bands support completely flat energy lines, which are extended over full BZ. Below we proceed with description of highly-symmetric points in terms of van Hove singularities in the DOS.

## III. SPECTRUM STRUCTURE AROUND HIGHLY-SYMMETRIC POINTS: VAN HOVE SINGULARITIES

Firstly, let us present general definitions that will be used throughout the text. By definition, the one-electron DOS per spin is given by

$$D(\varepsilon) = \sum_{i=1}^4 \int_{BZ} \frac{d^2k}{(2\pi)^2} \delta[\varepsilon - \varepsilon_i(\mathbf{k})], \quad (5)$$

with  $i$  running over the band dispersions  $\varepsilon_i(\mathbf{k})$  found from Eq.(3). Due to chiral symmetry the DOS is an even function of energy. The ordinary VHS with the logarithmic diverging DOS occurs at saddle point  $\mathbf{k}_s$  of a particular band in which

$$\nabla_{\mathbf{k}}\varepsilon(\mathbf{k}) = \mathbf{0} \text{ and } \det \mathcal{D} < 0, \quad (6)$$

where  $\mathcal{D}_{ij} \equiv \frac{1}{2}\partial_i\partial_j\varepsilon(\mathbf{k})$  is the  $2 \times 2$  Hessian matrix of a dispersion  $\varepsilon(\mathbf{k})$  at  $\mathbf{k}_s$ . Here and below we use shorthand notation  $\partial_i = \partial_{k_i}$ . After proper rotation of a basis,

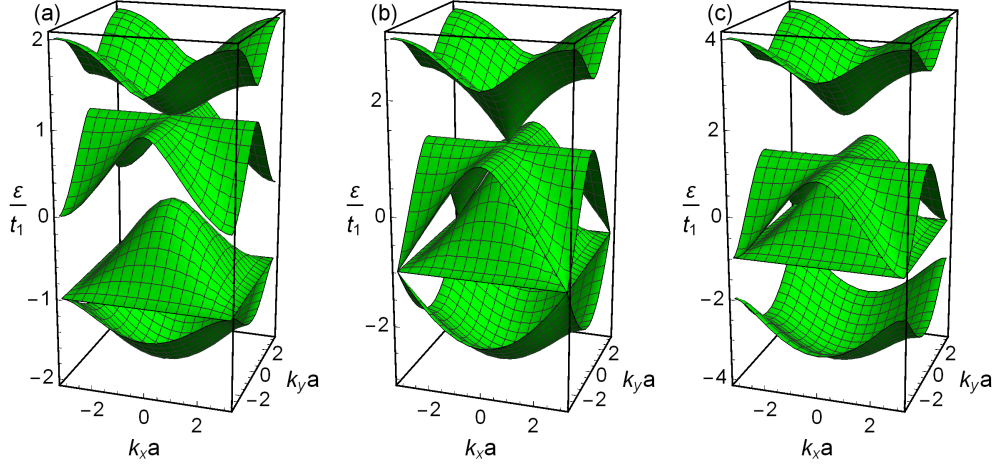


FIG. 2. Spectrum which is given by Eq.(3) for three values of parameter  $\alpha = t_2/t_1$ : panel (a)  $\alpha = \frac{1}{2}$ , panel (b)  $\alpha = 1$  and panel (c)  $\alpha = \frac{3}{2}$ . The energy  $E$  is measured in units of hopping parameter  $t_1$ . On the panel (b) one can observe the three-band touching points where the two Dirac cones meet nearly flat middle band.

the dispersion around saddle point can be conveniently represented as  $\varepsilon - \varepsilon_s \approx -\zeta p_x^2 + \beta p_y^2$  with wave vector deviation  $\mathbf{p} = \mathbf{k} - \mathbf{k}_s$ . The two coefficients  $\zeta$  and  $\beta$  are the eigenvalues of  $\mathcal{D}$  and satisfy the condition  $-\zeta\beta = \det \mathcal{D} < 0$ .

The high-order VHS corresponds to saddle point with the following properties [18]:

$$\nabla_{\mathbf{k}} \varepsilon = \mathbf{0} \text{ and } \det \mathcal{D} = 0. \quad (7)$$

This type can be divided into two types:  $\zeta = \beta = 0$  (multicritical VHS), or  $\zeta \neq 0, \beta = 0$ . The DOS is expected to have a power-law divergence at such points.

Below we perform expansion of the energy spectrum around highly-symmetric points and flat lines and identify the corresponding VHS type with the DOS divergence.

### A. $\Gamma$ and $M$ points

Before proceeding with calculation, we underline that previously mentioned symmetry of spectrum makes these two points equivalent up to change of energy sign. Thus, the analysis around the  $\Gamma$  point can be directly translated to the  $M$  point and vice versa by chiral symmetry.

To find the approximate expressions for band energies around highly-symmetric points, we perform the series expansion of spectral equation (3). We write  $\varepsilon = \varepsilon_i^{(0)} + \delta$ , with  $\varepsilon_i^{(0)}$  is the energy of  $i$ -th band exactly at the given point in  $\mathbf{k}$ -space. Then, we expand equation into series in  $\delta$  and  $\mathbf{k}a$  (measured from the given point), and find the solution for  $\delta$  in leading order. Performing this for  $\Gamma$

point, we find the following results in the case  $\alpha \neq 1$ :

$$\frac{\varepsilon_1}{t_1} \approx -1 - 2\alpha + \frac{\alpha|\mathbf{k}|^2 a^2}{4(\alpha + 1)}, \quad (8)$$

$$\begin{aligned} \frac{\varepsilon_{2,3}}{t_1} \approx & 1 + \frac{a^2 \alpha}{4(1 - \alpha^2)} \\ & \times \left[ \alpha|\mathbf{k}|^2 \pm \sqrt{(\alpha^2|\mathbf{k}|^4 + 4(1 - \alpha^2)k_x^2 k_y^2)} \right], \end{aligned} \quad (9)$$

$$\frac{\varepsilon_4}{t_1} \approx -1 + 2\alpha - \frac{\alpha|\mathbf{k}|^2 a^2}{4(1 - \alpha)}. \quad (10)$$

The numbering of bands goes from the lower one to the upper one. Also one should note that depending on sign of  $1 - \alpha$ , the indexes 2 and 4 should be interchanged (indexes in equations above work for  $\alpha > 1$ ). From expression (8) one can conclude that spectrum of tight-binding Hamiltonian (2) is bounded by  $-1 - 2\alpha < \varepsilon < 1 + 2\alpha$  at zero temperature. In particular, it follows from Eq.(9) that the top of band  $\varepsilon_3$  has completely flat lines along  $k_x$  and  $k_y$  axes.

In the case  $\alpha = 1$  we find the following expansions for three upper bands (which have triply degenerate point (see also Ref.[8])):

$$\begin{aligned} \frac{\varepsilon_1}{t_1} \approx & -3 + \frac{1}{8}a^2|\mathbf{k}|^2, \quad \frac{\varepsilon_3}{t_1} \approx 1 - \frac{k_x^2 k_y^2 a^2}{2|\mathbf{k}|^2}, \\ \frac{\varepsilon_{2,4}}{t_1} \approx & 1 \pm \frac{a}{\sqrt{2}}|\mathbf{k}| - \frac{a^2(k_x^2 - k_y^2)^2}{16|\mathbf{k}|^2}. \end{aligned} \quad (11)$$

The two bands  $\varepsilon_{2,4}$  form Dirac cones with Fermi velocity  $v_F = at_1/\sqrt{2}\hbar$  with additional square-order corrections in  $|\mathbf{k}|a$ . The middle band  $\varepsilon_3$  is completely flat in first-order approximation, but has nontrivial anisotropic corrections of second-order in  $|\mathbf{k}|a$ .

The  $\Gamma$  and  $M$  points define the energy boundaries of each band (see Fig.2). For  $\alpha \leq 1$  the bands are placed in

the ranges  $[-1-2\alpha, -1]$ ,  $[-1, -1+2\alpha]$ ,  $[1-2\alpha, 1]$ ,  $[1, 1+2\alpha]$  measured in units of  $t_1$ . It follows from the expansions (8)-(10) taken at  $\mathbf{k} = 0$ . We find that the gap near  $\varepsilon = 0$  opens for  $\alpha < 1/2$ . For the  $\alpha \geq 1$  the bands' energy ranges are  $\varepsilon/t_1 \in [-1-2\alpha, 1-2\alpha]$ ,  $[-1, 1]$  for both middle bands and  $[-1+2\alpha, 1+2\alpha]$ . In this case the gaps are opened for  $\alpha > 1$  above  $\varepsilon = t_1$  and below  $\varepsilon = -t_1$ , respectively. These features of spectrum are manifested in vanishing DOS in corresponding gap energy ranges, see Fig.3.

Next, we identify the type of VHS at  $\varepsilon_3 = t_1$  in  $\alpha = 1$  case. For this purpose, we evaluate the DOS contribution for each band separately, taking the leading term in wavevector expansion. The integration over wavevector in Eq.(5) is extended to cut-off parameter  $\Lambda$  of effective expansions (11). Then, the Dirac cones give the standard graphene-like result:

$$D_2(\varepsilon) + D_4(\varepsilon) = \frac{|\varepsilon - t_1|}{\pi a^2 t_1^2}. \quad (12)$$

The evaluation of DoS for middle nearly flat band is more complicated, at can be performed in polar coordinates  $k_x = k \cos \phi$  and  $k_y = k \sin \phi$ :

$$D_3(\varepsilon \lesssim t_1) = \int_0^\Lambda \int_0^{2\pi} \frac{k dk d\phi}{(2\pi)^2} \delta\left[\varepsilon - t_1 + t_1 \frac{k^2 a^2 \sin^2(2\phi)}{8}\right]. \quad (13)$$

We emphasize the fact that the middle band contributes only for  $\varepsilon < t_1$  and the corresponding DOS is asymmetric. The integration over  $k$  is easily performed, and the integration over angle can be confined to first quadrant with adding a total factor 4. Then, one should integrate in the limits where the solutions under delta-function are possible:

$$\begin{aligned} \phi_{min} &= \frac{1}{2} \arcsin\left(\sqrt{\frac{8(1-\varepsilon/t_1)}{\Lambda^2 a^2}}\right) < \phi < \\ \phi_{max} &= \frac{\pi}{2} - \frac{1}{2} \arcsin\left(\sqrt{\frac{8(1-\varepsilon/t_1)}{\Lambda^2 a^2}}\right). \end{aligned} \quad (14)$$

Thus, the integral for DOS becomes

$$\begin{aligned} D_3(\varepsilon \lesssim t_1) &= \frac{1}{t_1 a^2} \int_{\phi_{min}}^{\phi_{max}} d\phi \frac{4}{\sin^2(2\phi)} \\ &= \frac{4}{t_1 a^2} \sqrt{\frac{1}{x^2} - 1}, \quad x = \sqrt{\frac{8(1-\varepsilon/t_1)}{\Lambda^2 a^2}}. \end{aligned} \quad (15)$$

The total answer has the  $1/\sqrt{1-\varepsilon/t_1}$  divergence, as was noted previously:

$$\begin{aligned} D_3(\varepsilon \lesssim t_1) &= \frac{2}{t_1 a^2} \sqrt{\frac{\Lambda^2 a^2 - 8(1-\varepsilon/t_1)}{2(1-\varepsilon/t_1)}} \\ &\approx \frac{2}{t_1 a} \frac{\Lambda}{\sqrt{2(1-\varepsilon/t_1)}}. \end{aligned} \quad (16)$$

This power-law divergence together with asymmetry of the DOS clearly indicates, that this point corresponds to high-order VHS (see middle peaks of the DOS in all panels of Fig.3). Below we show that this holds true for all points on flat lines in dispersion. Also one should note that this singularity has larger exponent  $\kappa = 1/2$  (which is defined as  $D_3(\varepsilon \leq t_1) \sim |t_1 - \varepsilon|^{-\kappa}$ ) than in twisted bilayer graphene ( $\kappa = 1/4$ , [18]), and the same as in  $\text{Sr}_3\text{Ru}_2\text{O}_7$  [24] and  $\beta - \text{YbAlB}_4$  [25] materials.

Above we have found the long wavelength expansions of spectrum for small values of wavevector  $\mathbf{k}$ . However, these expansions are violated if the model parameter  $\alpha$  approaches 1. In this case we can use another series expansion of the spectrum: we assume that  $|1-\alpha| \sim |\mathbf{k}a|$  are of the same order. Then, we replace both expressions  $|1-\alpha|$  and  $|\mathbf{k}a|$  by ones multiplied by variable  $x$  in Eq.(3), and then expand the equation into powers of  $x$ . This guaranties that expansions keeps contributions from both small values  $|1-\alpha|$  and  $|\mathbf{k}a|$  in the same leading order. Next, we solve the approximate spectral equation around each band, as for Eqs.(8)-(10), and set  $x = 1$  in the final result. We find

$$\begin{aligned} \frac{\varepsilon_1}{t_1} &= -1 - 2\alpha + \frac{(k_x^2 + k_y^2)a^2}{8}, \quad \frac{\varepsilon_3}{t_1} = 1 - \frac{k_x^2 k_y^2 a^2}{2(k_x^2 + k_y^2)}, \\ \frac{\varepsilon_{2,4}}{t_1} &= 1 - \left( (1-\alpha) \pm \sqrt{\frac{(k_x^2 + k_y^2)a^2}{2} + (1-\alpha)^2} \right). \end{aligned} \quad (17)$$

The last two expressions show that the  $|1-\alpha|$  competes with  $|\mathbf{k}|a$  and their larger value defines the spectrum form in the leading order.

## B. X-points and flat lines

At  $X$  point the eigenvalues of Hamiltonian (2) are

$$\varepsilon_{1,4}^X = \mp t_1 \sqrt{1 + 4\alpha^2}, \quad \varepsilon_{2,3}^X = \mp t_1. \quad (18)$$

The  $\varepsilon_{1,4}$  represent dispersion of upper and lower bands, respectively. The dispersions  $\varepsilon_{2,3}$  correspond to flat lines for the points in  $k$ -space, which are situated in the middle between band-touching points. In Appendix A we show how the flat lines are related to the  $C_4$  point symmetry group of the lattice and structure of tight-binding Hamiltonian. Performing the series expansion of spectral equation in the same way as discussed above Eq.(8) but for wavevectors around  $X = (0, \frac{\pi}{a})$ , we find:

$$\begin{aligned} \varepsilon_1 &\approx \varepsilon_1^X + \frac{t_1 a^2}{4} \left[ k_x^2 \left( 1 + \frac{t_1}{\varepsilon_1^X} \right) - \left( k_y - \frac{\pi}{a} \right)^2 \left( 1 - \frac{t_1}{\varepsilon_1^X} \right) \right], \\ \varepsilon_4 &= \varepsilon_4^X + \frac{t_1 a^2}{4} \left[ k_x^2 \left( 1 + \frac{t_1}{\varepsilon_4^X} \right) - \left( k_y - \frac{\pi}{a} \right)^2 \left( 1 - \frac{t_1}{\varepsilon_4^X} \right) \right]. \end{aligned} \quad (19)$$

These two dispersion relations represent ordinary VHS, defined via the conditions (6). The Hessian matrix is



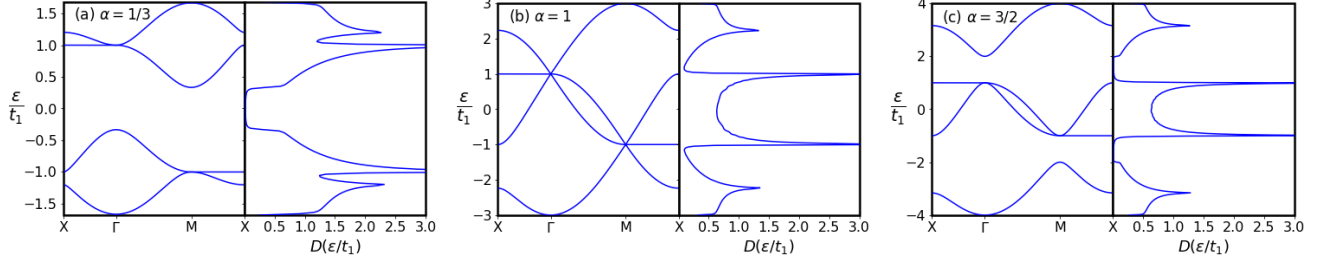


FIG. 3. The spectrum of  $T$ -graphene along the closed path  $X - \Gamma - M - X$  and DOS for  $\alpha = 1/3, 1$  and  $\alpha = 3/2$ . DOS is plotted on the right of each spectrum, and is measured in units of  $\frac{1}{a^2 t_1}$ . DOS is regularized with finite broadening of levels,  $\Gamma = 0.01 t_1$  to make plots smooth.

diagonal and its' elements are the derivatives of above dispersion relations with respect to wavevectors,  $\mathcal{D} = \text{diag}(\partial_{xx}\varepsilon, \partial_{yy}\varepsilon)$ . The DOS exhibits a logarithmic divergence around  $\varepsilon = \varepsilon_1^X$  and  $\varepsilon = \varepsilon_4^X$ :  $D_{1,4}(\varepsilon) \sim \log\left(\frac{\Lambda a^2 t_1}{|\varepsilon - \varepsilon_{1,4}^X|}\right)$ . These upper and lower peaks in DOS are clearly visible on Fig.3.

Next, we find the series expansion of  $\varepsilon_{2,3}$  bands' dispersion around  $X$  point. Due to chiral symmetry mentioned after Eq.(3), it suffices to make expansion only for upper band, while for lower band it can be found by appropriate change of wavevectors. Expanding the spectral equation (3) for third band around energy  $\varepsilon_3 = t_1$  into series in  $k_x a$ , we find:

$$\varepsilon_3 \approx t_1 - t_1 \left[ \frac{k_x^2 a^2}{2} - \frac{k_x^4 a^4}{24} - \frac{k_x^4 a^4}{4(1 - \cos(k_y a))} \right]. \quad (21)$$

Here we used the same method of searching approximate dispersion as for Eqs.(8)-(10). This approximation works well only for  $\frac{k_x^4 a^4}{4(1 - \cos(k_y a))} < \frac{k_x^2 a^2}{2}$ , since this band has  $\varepsilon_3 \leq t_1$  energy for all points in BZ. The Hessian matrix for the dispersion (21) has only one nonzero component on diagonal  $\mathcal{D} = \text{diag}\left(-\frac{t_1 a^2}{2}, 0\right)$ . Thus, we observe that the middle bands at  $X$ -point and in other points of flat line where  $1 - \cos(k_y a) \neq 1$  exhibit a high-order saddle point. Since we have already checked that in  $\Gamma$  and  $M$  points the van Hove singularity is of the high-order, we conclude that flat lines consist of high-order singular saddle points. This can be clearly understood from the 3D plots of spectrum, which are presented on Fig.2. One can check that the DOS for dispersion (21) has a inverse square root divergence  $1/\sqrt{t_1 - \varepsilon}$  with energy, with benchmark asymmetry:

$$\begin{aligned} D_3(\varepsilon \lesssim t_1) &= \int \frac{d^2 k}{(2\pi)^2} \delta\left[\varepsilon - t_1 \left(1 - \frac{k_x^2 a^2}{2}\right)\right] \\ &= \frac{\Lambda}{\sqrt{2}\pi^2 a t_1 \sqrt{1 - \varepsilon/t_1}}. \end{aligned} \quad (22)$$

In Fig.3 we present dispersion relations for  $T$ -graphene along the path  $X - \Gamma - M - X$  which represents the main features in spectrum (left part of each panel) and

DOS (regularized by finite level broadening, right part of each panel) for the values  $\alpha = 1/3, 1$  and  $\alpha = 3/2$ . Note that the path length in  $M - \Gamma$  direction is  $\sqrt{2}$  times large than in  $X - M$  or  $\Gamma - X$  directions. Our plots show that at energies  $\pm t_1 \sqrt{1 + 4\alpha^2}$  DOS exhibits logarithmic divergences, which are the standard VHS at  $X$  points. At the same time, the much stronger peaks in DOS correspond to flat lines in spectrum at energies  $\pm t_1$  which are 'high-order' VHS. Our results for spectra agree with the results of Refs.[6–8].

Fig.3 demonstrates also evolution of DOS as the function of the hoppings ratio  $\alpha$ . At  $\varepsilon = 0$  we find that for  $\alpha < 1/2$  there are no states (insulating phase), while for larger  $\alpha$  the states are present. For energies  $|\varepsilon| < t_1$  the DOS is always finite for  $\alpha > 1/2$  meaning metallic behavior. On the other hand, for energies  $|\varepsilon| > t_1$  and  $\alpha > 1$  we observe the presence of gaps in the DOS.

In Sec.IV we will study the behavior of orbital susceptibility around van Hove singularities.

### C. Effective models of band touching point: linear and quadratic approximations

In the tight-binding model of square-octagon lattice the band touching exists at two highly-symmetric points -  $\Gamma$  and  $M$ . Since they are related by chiral symmetry (see discussion after Eq.(3)), we need to build an effective Hamiltonian only at one of these points. As was proposed in Ref.[8], one can perform a rotation to  $C_{4v}$  basis which is defined through four linear combinations of wave function components

$$\begin{aligned} |A_1\rangle &= \frac{1}{2} (c_A^\dagger + c_B^\dagger + c_C^\dagger + c_D^\dagger) |0\rangle, \\ (|E_x\rangle, |E_y\rangle) &= \frac{1}{\sqrt{2}} (c_A^\dagger - c_C^\dagger, c_B^\dagger - c_D^\dagger) |0\rangle, \\ |B_1\rangle &= \frac{1}{2} (c_A^\dagger - c_B^\dagger + c_C^\dagger - c_D^\dagger) |0\rangle, \end{aligned} \quad (23)$$

where  $c_i^\dagger$  are the on-site electron creation operators. After such unitary transformation we obtain the following first-

order effective  $SU(3)$  Hamiltonian near the  $\Gamma$  point:

$$H_{SU(3)} = t_1 \begin{pmatrix} 1 & 0 & -\frac{iak_x}{\sqrt{2}} \\ 0 & 1 & \frac{iak_y}{\sqrt{2}} \\ \frac{iak_x}{\sqrt{2}} & -\frac{iak_y}{\sqrt{2}} & 2\alpha - 1 \end{pmatrix}. \quad (24)$$

This Hamiltonian is useful for understanding how the Dirac cones emerge in spectrum for  $\alpha = 1$ . The spectrum defined by this Hamiltonian is

$$\frac{\varepsilon_0}{t_1} = 1, \quad \frac{\varepsilon_{\pm}}{t_1} = \alpha \pm \sqrt{\frac{a^2|\mathbf{k}|^2}{2} + (\alpha - 1)^2}. \quad (25)$$

The corresponding eigenvectors are

$$\begin{aligned} \Psi_0 &= \frac{1}{|\mathbf{k}|} (k_y, k_x, 0), \\ \Psi_- &= \frac{(ik_x a, -ik_y a, \sqrt{2}(1 - \varepsilon_-))}{\sqrt{2}(|\mathbf{k}|^2 a^2 + 2(1 - \alpha)(1 - \varepsilon_-))}, \\ \Psi_+ &= \frac{(-ik_x a, ik_y a, \sqrt{2}(\varepsilon_+ - 1))}{\sqrt{2}(|\mathbf{k}|^2 a^2 + 2(\alpha - 1)(\varepsilon_+ - 1))}. \end{aligned} \quad (26)$$

One should note that the linear Hamiltonian of such type does not capture the spectral structure of middle band. Instead, the middle band is treated as completely flat, and the corresponding effective theory is an example of pseudospin-1 fermion models (see Ref.[32] for topological classification of such theories). Since the aim of present paper is to analyze the role of high-order VHS, we need to build the effective Hamiltonian that correctly captures the dispersion of middle band at leading order in  $|\mathbf{k}|a$ . The needed dispersion is presented, for example, in Eq.(11) in the  $\alpha = 1$  case.

To find corresponding effective Hamiltonian, we use Lödwin method [33], which is also called Lödwin partitioning (the example calculation for Lieb-kagome Hamiltonian was performed in Ref.[34]). The idea is to decompose the full tight-binding Hamiltonian after rotation from Ref.[8] into blocks:

$$H = \begin{pmatrix} H_{\alpha\alpha} & H_{\alpha\beta} \\ H_{\beta\alpha} & H_{\beta\beta} \end{pmatrix}, \quad (27)$$

where the  $\alpha$  subspace describes  $SU(3)$  band-touching and  $\beta$  subspace corresponds to lower band, decoupled from other three bands by relatively large gap. Then, the effective second-order Hamiltonian around band-touching is written as

$$H_{\alpha} = H_{\alpha\alpha} + H_{\alpha\beta} (\varepsilon_0 - H_{\beta\beta})^{-1} H_{\beta\alpha}, \quad (28)$$

where  $\varepsilon_0 = \varepsilon_{2,3}(\mathbf{k} = 0) = t_1$ . For  $\Gamma$  point this Hamiltonian has the following form

$$H_{SU(3)}^{(2)} = \hat{\varepsilon}^{(0)} + t_1 \begin{pmatrix} -\frac{a^2(2\alpha+1)k_x^2}{4(\alpha+1)} & \frac{a^2 k_x k_y}{4\alpha+4} & -\frac{iak_x}{\sqrt{2}} \\ \frac{a^2 k_x k_y}{4\alpha+4} & -\frac{a^2(2\alpha+1)k_y^2}{4(\alpha+1)} & \frac{iak_y}{\sqrt{2}} \\ \frac{iak_x}{\sqrt{2}} & -\frac{iak_y}{\sqrt{2}} & \frac{k^2 a^2}{4} \end{pmatrix}, \quad (29)$$

where  $\hat{\varepsilon}^{(0)} = t_1 \text{diag}(1, 1, 2\alpha - 1)$ . Such simple Hamiltonian is particularly useful when the proper dispersion of all three bands is needed at leading order.

#### IV. ORBITAL SUSCEPTIBILITY

The susceptibility measures the response of a electronic system to an external magnetic field and is defined standardly as the second derivative of the grand canonical potential at zero field. In this section we discuss the numerical approach for evaluating the orbital susceptibility. The main formula, which is most suitable in our case for numerical calculation, was given in Ref.[35], the more general formula was derived in Ref.[30]. The susceptibility can be represented as

$$\chi_{\text{orb}}(\mu, T) = -\frac{\mu_0 e^2}{12\hbar^2} \frac{\text{Im}}{\pi S} \int_{-\infty}^{\infty} n_F(\varepsilon) \text{Tr} \hat{X} d\varepsilon. \quad (30)$$

Here  $n_F(\varepsilon) = 1/(e^{(\varepsilon-\mu)/T} + 1)$  is the Fermi distribution,  $\mu_0 = 4\pi \times 10^{-7}$  in SI units and  $S$  is the area of the sample. The trace contains the integral over the BZ and the trace over band indices:

$$\text{Tr}(\bullet) = \sum_{\mathbf{k}} \text{tr}(\bullet) = S \int_{\text{BZ}} \frac{d^2 k}{4\pi^2} \text{tr}(\bullet). \quad (31)$$

The operator  $\hat{X}$  is written in terms of zero-field Green function  $G(\mathbf{k})$  and Bloch Hamiltonian  $H(\mathbf{k})$ , and  $\partial_{x,y}$  are partial derivatives over momenta:

$$\begin{aligned} \hat{X} &= G(\mathbf{k}) \partial_x^2 H(\mathbf{k}) G(\mathbf{k}) \partial_y^2 H(\mathbf{k}) - \\ &- G(\mathbf{k}) \partial_{xy}^2 H(\mathbf{k}) G(\mathbf{k}) \partial_{xy}^2 H(\mathbf{k}) + \\ &+ 2([G(\mathbf{k}) \partial_x H(\mathbf{k}), G(\mathbf{k}) \partial_y H(\mathbf{k})])^2. \end{aligned} \quad (32)$$

The orbital susceptibility can be rewritten in several other forms, one of them without commutator [30],

$$\begin{aligned} \chi_{\text{orb}}(\mu, T) &= -\frac{\mu_0 e^2}{12\hbar^2} \frac{\text{Im}}{\pi S} \int_{-\infty}^{+\infty} n_F(\varepsilon) \text{Tr} \{GH^{xx}GH^{yy} \\ &- GH^{xy}GH^{xy} - 4(GH^x GH^x GH^y GH^y \\ &- GH^x GH^y GH^x GH^y)\} d\varepsilon. \end{aligned} \quad (33)$$

Here  $G = G(\mathbf{k})$  is the Green function and  $H^i, H^{ij}$  denote the first and second derivatives of Hamiltonian with respect to components of momenta  $k_{i,j}$  and the trace contains momenta integration, as defined below (31). The last formula can be also rewritten [30] in terms of previously found one by Gomez-Santos [29],

$$\begin{aligned} \chi_{\text{orb}}(\mu, T) &= -\frac{\mu_0 e^2}{2\hbar^2} \frac{\text{Im}}{\pi S} \int_{-\infty}^{+\infty} n_F(\varepsilon) \text{Tr} \{GH^x GH^y GH^x \\ &\times GH^y + \frac{1}{2}(GH^x GH^y + GH^y GH^x) GH^{xy}\} d\varepsilon. \end{aligned} \quad (34)$$

Here the first term represents the Fukuyama result [36]. Three formulas for susceptibility are equivalent of course,

but the expressions under traces do not coincide. The use of a specific formula depends on possible simplifications, for example, for Hamiltonians linear in momenta the expressions (32) or (33) are preferred since the terms with second derivatives  $H^{ij}$  vanish.

To check the numerical results below we can use the sum rule that the integral of the orbital susceptibility over the whole band vanishes:

$$\int \chi_{\text{orb}}(\mu, T) d\mu = 0. \quad (35)$$

The derivation of sum rule for general tight-binding model was given in Ref.[37]. Below we apply the formulas for orbital susceptibility to particular models, namely - tight-binding model of tetragraphene and effective low-energy  $SU(3)$  model.

### A. Application of general formulas to tetragraphene

Let us now apply the formula (30) to tetragraphene Hamiltonian (2). Since the second derivatives  $\partial_{xy}^2 H$  and  $\partial_{yx}^2 H$  vanish, the operator  $\hat{X}$  reduces to

$$\hat{X} = G(\mathbf{k})\partial_x^2 H(\mathbf{k})G(\mathbf{k})\partial_y^2 H(\mathbf{k}) + 2([G(\mathbf{k})\partial_x H(\mathbf{k}), G(\mathbf{k})\partial_y H(\mathbf{k})])^2. \quad (36)$$

The Green's function is given in Appendix B. Then, calculating the trace of  $\hat{X}$  for each term separately, we find:

$$\text{tr} [\text{term 1}] = \frac{a^4}{\det[\varepsilon - \frac{1}{t_1}H(\mathbf{k})]^2} \left[ 4\alpha^2 ((\varepsilon^2 + 1) \cos(k_x a) - 2\varepsilon) ((\varepsilon^2 + 1) \cos(k_y a) - 2\varepsilon) \right], \quad (37)$$

$$\begin{aligned} \text{tr} [\text{term 2}] = & \frac{16\alpha^2 a^4}{\det[\varepsilon - \frac{1}{t_1}H(\mathbf{k})]^3} \left[ t_1^2 \alpha^2 (\varepsilon^2 + 2)^2 + \varepsilon (\alpha^2 \varepsilon (\varepsilon^2 + 2) \cos(2k_x a) + ((\varepsilon^2 - 1)^2 - 4\varepsilon^2 \alpha^2 (\varepsilon^2 + 2)) \cos(k_x a)) \right. \\ & + 2\alpha^2 \varepsilon^2 \cos(2k_y a) (\varepsilon \cos(k_x a) - 1)^2 + \cos(k_y a) (-2(2\alpha^2 + 1)\varepsilon^3 - 8\alpha^2 \varepsilon - 4\alpha^2 \varepsilon^3 \cos(2k_x a) \\ & \left. + (4\alpha \varepsilon - \varepsilon^2 + 1)(4\alpha \varepsilon + \varepsilon^2 - 1) \cos(k_x a) + \varepsilon^5 + \varepsilon) - \varepsilon^2 (\varepsilon^2 - 1)^2 \right]. \end{aligned} \quad (38)$$

We denote the first term with second derivatives in (36) as term 1 and the term with commutator as term 2. Here and thereafter we use dimensionless energy parameter  $\varepsilon \rightarrow \varepsilon/t_1$  to simplify the form of expressions. Note that both determinants in denominators come from Green function. Also one should notice that the numerators in both terms are real, thus the imaginary part comes fully from integration over energy due to the presence of singular denominators. We write the determinants as  $\prod_{i=1}^4 (\varepsilon - \varepsilon_i(\mathbf{k}))$ , where  $\varepsilon_i(\mathbf{k})$  are band energies measured in units of  $t_1$ .

One can use also an alternative expression (34) for susceptibility obtaining shorter expression

$$\begin{aligned} \chi_{\text{orb}}(\mu, T) = & -\frac{\mu_0 e^2 t_1}{2\hbar^2} \frac{\text{Im}}{\pi} \int_{-\infty}^{+\infty} d\varepsilon n_F(t_1 \varepsilon) \\ & \times \int_{BZ} \frac{d^2 k}{4\pi^2} \text{tr} \{GH^x GH^y GH^x GH^y\}. \end{aligned} \quad (39)$$

Evaluating the trace, we find

$$\begin{aligned} \text{tr} \{GH^x GH^y GH^x GH^y\} \\ = \left( \frac{2\alpha a(\varepsilon^2 - 1)}{\det[\varepsilon - \frac{1}{t_1}H(\mathbf{k})]} \right)^4 \sin^2(k_x a) \sin^2(k_y a). \end{aligned} \quad (40)$$

The advantage of this formula is that the numerator is much simpler comparing to Eqs.(37)-(38). However, the larger power of denominator makes it harder to perform numerical calculation, since the behavior at band-touching point is more singular.

The integrals over energy can be evaluated analytically using Cauchy formula with residues. Next, we need to calculate the integrals over wavevector in full BZ. They are cumbersome and can be performed only numerically.

The numerical evaluation can be performed by sampling many points in BZ, and replacing integral by a quadrature sum. For this purpose we use Monte Carlo approach - it converges very fast with increasing number of sample points for multidimensional integrals. Taking  $N$  sample points in BZ, the integral over  $d^2 k$  is replaced by the sum  $\int_{BZ} \frac{d^2 k}{(2\pi)^2} f(\mathbf{k}) = \frac{1}{N} \sum_j f(\mathbf{k}_j)$ . Then, the final

formula used in evaluation is

$$\chi_{\text{orb}}(\mu, T) = \frac{\chi_0}{N} \sum_{j=1}^N \left[ \sum_i \text{res}_{\varepsilon=\varepsilon_i} n_F(t_1 \varepsilon) f^R(\varepsilon) \right]_{\mathbf{k}=\mathbf{k}_j}. \quad (41)$$

The residues were evaluated analytically using expressions (37)-(38), and the band energy solutions of spectral equation (3) were substituted numerically into final rather cumbersome expressions. Here we introduced the scale factor for susceptibility  $\chi_0 = \mu_0 e^2 a^2 t_1 / 12 \hbar^2$ .

The results of evaluation for  $\chi$  as a function of chemical potential are shown in Fig.4. We have checked that good convergence is reached for  $N = 10^5$  and  $N = 5 \times 10^5$  for the first and second terms, respectively. The errors of integration become in this case several orders less than the absolute values of susceptibility. As a test, we checked that the sum rule, which is given by Eq.(35), holds true with the same precision.

The orbital susceptibility exhibits standard weak diamagnetic peaks near the edges of the spectrum, which can be easily understood from Landau-Peierls formula [30, 35, 38, and 39],

$$\chi_{\text{LP}}(\mu, T) = \frac{\mu_0 e^2}{12 \hbar^2} \sum_{i=1}^4 \int \frac{d^2 k}{4 \pi^2} n'_F(\varepsilon_i) (\partial_x^2 \varepsilon_i \partial_y^2 \varepsilon_i - \partial_{xy}^2 \varepsilon_i \partial_{xy}^2 \varepsilon_i), \quad (42)$$

which takes into account only intraband contributions. Here  $n'_F(\varepsilon)$  is a derivative of the Fermi distribution function. In the case of T-graphene only the lower (upper) band gives strong contribution to the orbital susceptibility at the lower (upper) edge of the spectrum. This can be clearly seen from Figs.2 and 3, since at lower (upper) edge the corresponding band in  $\Gamma$  (M) point is separated by a large gap from other three bands. The dispersion of this band is quadratic in momenta, see Eq.(8), and both derivatives in first term of LP formula are positive. The second term exactly vanishes, and thus the total susceptibility is negative because  $n'_F(\varepsilon) < 0$ . These peaks are clearly visible in all panels of Fig.4.

At the ordinary van Hove points, which are placed on upper and lower bands at X-points at the energy

levels  $\varepsilon_{1,4}^X = \mp \sqrt{1 + 4\alpha^2}$ , one finds strong paramagnetic peaks. These peaks are also well-described by the Landau-Peierls formula (42). Substituting series expansion (19) or (20), one finds that only the first term in Landau-Peierls formula is nonzero, and have positive sign due to opposite signs of  $\partial_x^2$  and  $\partial_y^2$  derivatives. Moreover, due to the divergent DOS at this energy level, the contribution of this band dominates and leads to strong paramagnetism. This is also related to famous magnetic breakdown phenomena [40], where the quasiclassical approximation in terms of electronic orbits fails in the vicinity of saddle points due to effects of tunneling from one trajectory to the neighboring one that leads to rotation of the electron in a direction opposite to the direction of classical rotation (see Ref.[19] for physical picture of this phenomenon).

Near the energy levels  $\mu = \pm t_1$  (see Fig.4) we find strong paramagnetic and diamagnetic peaks, the amplitude of which strongly depends on tight-binding parameter  $\alpha$ . The existence of the orbital paramagnetism is a necessary condition to cancel the diamagnetic contribution in order to satisfy the sum rule (35).

Below we analyze the orbital susceptibility for effective linear Hamiltonian to obtain some insights into the physics of these peculiar features. Also, we find numerically the presence of dia- paramagnetic phase transition at such energy levels, which is discussed below.

## B. Analytical results in effective pseudospin-1 model around band-touching

Let us use the linear effective Hamiltonian around band-touching point to find an analytical approximation for the susceptibility. It is given by Eq.(24), and we omit the dimensional parameter  $t_1$ , restoring it in the final expressions for susceptibility,

$$H_3 \equiv \frac{H_{SU(3)}}{t_1} = \begin{pmatrix} 1 & 0 & -\frac{ia k_x}{\sqrt{2}} \\ 0 & 1 & \frac{ia k_y}{\sqrt{2}} \\ \frac{ia k_x}{\sqrt{2}} & -\frac{ia k_y}{\sqrt{2}} & 2\alpha - 1 \end{pmatrix}. \quad (43)$$

The corresponding Green function is

$$G_{SU(3)} = \frac{1}{\det[\varepsilon - H_3]} \begin{pmatrix} \varepsilon^2 - \frac{1}{2}a^2 k_y^2 - 2\alpha(\varepsilon - 1) - 1 & -\frac{1}{2}a^2 k_x k_y & -\frac{ia(\varepsilon-1)k_x}{\sqrt{2}} \\ -\frac{1}{2}a^2 k_x k_y & \varepsilon^2 - \frac{1}{2}a^2 k_x^2 - 2\alpha(\varepsilon - 1) - 1 & \frac{ia(\varepsilon-1)k_y}{\sqrt{2}} \\ \frac{ia(\varepsilon-1)k_x}{\sqrt{2}} & -\frac{ia(\varepsilon-1)k_y}{\sqrt{2}} & (\varepsilon - 1)^2 \end{pmatrix}. \quad (44)$$

The determinant in denominator is simple and gives two Dirac cones and flat band

$$\det[\varepsilon - H_3] = \frac{1 - \varepsilon}{2} (a^2 \mathbf{k}^2 + 2(\varepsilon - 1)(2\alpha - \varepsilon - 1)). \quad (45)$$

The first derivatives of Hamiltonian are,

$$H_3^x = \frac{a}{\sqrt{2}} \begin{pmatrix} 0 & 0 & -i \\ 0 & 0 & 0 \\ i & 0 & 0 \end{pmatrix}, \quad H_3^y = \frac{a}{\sqrt{2}} \begin{pmatrix} 0 & 0 & 0 \\ 0 & 0 & i \\ 0 & -i & 0 \end{pmatrix}, \quad (46)$$



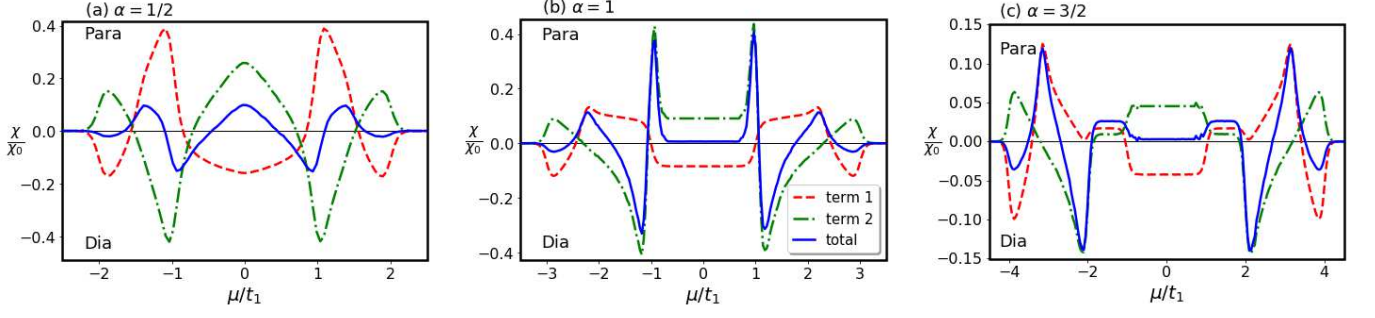


FIG. 4. The dependence of susceptibility on chemical potential, measured in units of  $t_1$  hopping parameter, for three values of  $\alpha$ :  $1/2, 1, 3/2$ . The legend on panel (b) shows the lines definitions: dashed and dash-dotted lines correspond to first and second term contributions in  $\hat{X}$  (see Eq.(36)), while the solid line describes the total susceptibility. The full spectrum is bounded by values  $-1 - 2\alpha < \varepsilon < 1 + 2\alpha$  and the orbital susceptibility vanishes outside these energies.

while all second derivatives are zero. Then, we can apply the formula (34), which in our case reduces to

$$\chi_{\text{orb}}(\mu, T) = -\frac{\mu_0 e^2 t_1}{2\hbar^2} \times \frac{\text{Im}}{\pi S} \int_{-\infty}^{+\infty} n_F(\varepsilon) \text{Tr} \{GH^x GH^y GH^x GH^y\} d\varepsilon. \quad (47)$$

Calculating the matrix trace we come at the orbital susceptibility given by the triple integral,

$$\chi_{\text{orb}}(\mu, T) = -\frac{\mu_0 e^2 t_1}{2\hbar^2} \frac{\text{Im}}{\pi} \int_{-\infty}^{+\infty} n_F(t_1 \varepsilon) d\varepsilon \times \int \frac{d^2 k}{4\pi^2} \frac{16a^8 k_x^2 k_y^2}{(a^2(k_x^2 + k_y^2) + 2(\varepsilon - 1)(2\alpha - \varepsilon - 1))^4}. \quad (48)$$

The integration over momenta is easily performed using polar coordinates

$$\begin{aligned} & \int \frac{d^2 k}{4\pi^2} \frac{16a^8 k_x^2 k_y^2}{(a^2(k_x^2 + k_y^2) + 2(\varepsilon - 1)(2\alpha - \varepsilon - 1))^4} \\ &= \frac{a^2}{12\pi} \times \begin{cases} \frac{1}{2(\alpha-1)} \left( \frac{1}{\varepsilon-1} - \frac{1}{\varepsilon+1-2\alpha} \right), & \alpha \neq 1, \\ -\frac{1}{(\varepsilon-1)^2}, & \alpha = 1. \end{cases} \end{aligned} \quad (49)$$

Then, using the formula

$$\text{Im} \int_{-\infty}^{+\infty} \frac{f(E)}{(E - \alpha)^j} dE = -\frac{\pi}{(j-1)!} f^{(j-1)}(\alpha), \quad (50)$$

for susceptibility we finally obtain:

$$\begin{aligned} \chi_{\text{orb}}(\mu, T) &= -\frac{\chi_0}{2\pi} \\ &\times \begin{cases} \frac{1}{2(\alpha-1)} (n_F(t_1(2\alpha-1)) - n_F(t_1)), & \alpha \neq 1, \\ t_1 n'_F(t_1), & \alpha = 1. \end{cases} \end{aligned} \quad (51)$$

Note that the case  $\alpha = 1$  is the limit of upper case  $\alpha \neq 1$ . These results are similar to graphene. Note however, that

this theory does not capture the correct dispersion of the middle band.

The plot of effective susceptibility defined by Eq.(51) is shown in Fig.5. We compare its dependence on  $\alpha$  with total susceptibility evaluated numerically. The doping level  $\mu = t_1$  coincides with the band touching point at which the high-order VHS and Dirac point are present for  $\alpha = 1$ . Below we discuss this transition in more detail.

### C. Paramagnetic-diamagnetic phase transition at band-touching point

At the Fermi level  $\mu = 0$  the orbital susceptibility does not exhibit any peculiar properties. However, when the doping is tuned to band-touching point  $\mu = t_1$ , one can expect nontrivial behavior of susceptibility due to presence of massless fermions forming a Dirac cone and flat lines with high-order VHS of DOS. To check the properties of system at such doping level, we calculate the orbital susceptibility as a function of hopping ratio  $\alpha = t_2/t_1$ . The results are plotted in Fig.5 and compared with results for effective  $SU(3)$  low-energy theory. An important physical finding represented in above data is a diamagnetic-paramagnetic phase transition. It was not captured by the effective theory (see Eq.(51)), because such transition is a result of interplay of all four bands. Numerically we find that the dia-paramagnetic transition occurs at  $\alpha \approx 0.94$ .

Qualitatively, one can expect that such transition occurs due to the presence of Dirac cones, which give strong diamagnetism in graphene [30 and 41] and a high-order VHS, that should result in strong paramagnetism. The competition between these two opposite responses together with the weak role of fourth band leads to dia-paramagnetic transition.

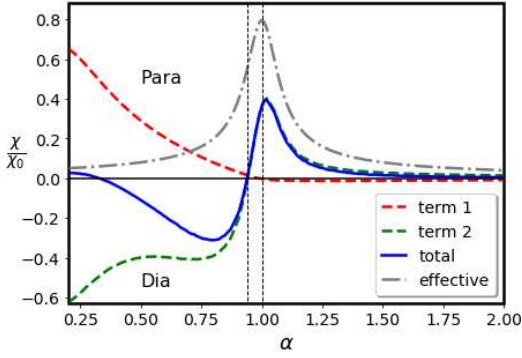


FIG. 5. The dependence of orbital susceptibility on relative strength of tight-binding parameters  $\alpha = t_2/t_1$  for  $\mu = 1.0t_1$  and  $T = 0.05t_1$ . The numerically-evaluated total susceptibility (solid blue line) is compared with susceptibility obtained from effective pseudospin-1 Hamiltonian (24) (gray dash-dotted line). Red and green dash lines represent separate contributions due to terms (37) and (38), respectively.

## V. CONCLUSIONS

In this paper we have studied the spectrum structure of tight-binding model for square-octagon lattice and analyzed the emergence of Dirac cones and van Hove singularities of different type. Firstly, we found that the singularities in DOS, that correspond to the flat lines in spectrum of T-graphene, represent VHS of high-order. Their benchmarks are large divergence exponent  $\kappa = 1/2$  (instead of logarithmic divergence for ordinary VHS) and asymmetry of DOS near corresponding energy level. Such high-order saddle points in spectrum are intermediate between the ordinary saddle points and completely flat bands. Also, using the Lödwin partitioning, we determined an effective second-order Hamiltonian that correctly captures dispersions of three bands near the high-order saddle point.

Secondly, we have studied the orbital susceptibility of electrons on square-octagon lattice. We have found that while for ordinary VHS there are standard paramagnetic peaks predicted long ago by Vignale [19], the recently introduced high-order VHS [18] manifest themselves in a more complicated way.

Studying the orbital susceptibility at band-touching point as a function of tight-binding hoppings ratio  $\alpha$ , we found a diamagnetic-paramagnetic transition at  $\alpha \approx 0.94$ . Its existence can be qualitatively understood due to competitions of contributions from Dirac cones, which give strong diamagnetism, and high-order VHS that result in strong paramagnetism. The tight-binding parameter  $\alpha$  can be varied due to in-plane deformations allowing to verify the dia- paramagnetic transition in experiment. Though it is not probably easy to fine-tune the hopping parameters experimentally, one can observe the different phases by analyzing different materials that are based on square-octagon lattice (see Refs. [13 and 17]). The effective low-energy pseudospin-1 Hamiltonian

near the  $\Gamma$  point (24) correctly describes paramagnetic contribution but does not capture the dia-paramagnetic transition.

Let us discuss the role of van Hove singularities in T-graphene. For the ordinary VHS the orbital susceptibility exhibits paramagnetic peak [19]. This can be understood using the standard Landau-Peierls formula for contribution of single band [30]. In T-graphene, at the doping level  $\mu = \pm t_1$ , one meets the high-order VHS in dispersion as well as three band touching point, two of which are Dirac cones. In a single-layer graphene the presence of Dirac cones leads to singular diamagnetic contribution into orbital susceptibility  $\chi \sim -\chi_0\delta(\mu)$  at zero temperature [41]. In the case of T-graphene, the presence of highly-degenerate middle band leads to competing strong paramagnetic contribution, resulting in sign change of orbital susceptibility. One should expect the manifestation of high-order van Hove singularities of T-graphene also in other physical quantities besides orbital susceptibility. Finally, we note that the accessibility of doping levels beyond the van Hove singularity was demonstrated in recent experiment for single-layer graphene [42].

## ACKNOWLEDGMENTS

We are grateful to E.V. Gorbar for useful remarks. The work of V.P.G. is supported by the National Research Foundation of Ukraine grant "Topological phases of matter and excitations in Dirac materials, Josephson junctions and magnets". V.M.L. acknowledges collaboration within the Ukrainian-Israeli Scientific Research Program of the Ministry of Education and Science of Ukraine (MESU) and the Ministry of Science and Technology of the state of Israel (MOST).

### Appendix A: Flat lines in dispersion of middle bands and lattice symmetry

In this Appendix we show that the flat lines in spectrum are related to the  $C_4$  point symmetry group. Firstly, one can check that setting  $k_x a = 0$  or  $k_y a = 0$  in spectral equation (3), it can be factorized:

$$(\varepsilon + 1) \left( - (4\alpha^2 + 1) \varepsilon + 4\alpha^2 \cos(ak_y) + \varepsilon^3 - \varepsilon^2 + 1 \right) = 0. \quad (\text{A1})$$

Here we used scaled energy parameter  $\varepsilon$ , measured in units of  $t_1$ . Thus, we find the middle band dispersion  $\varepsilon = -1$ , which describes a flat line. The same property of spectral equation holds true for  $k_x a = \pm\pi$  and  $k_y a = \pm\pi$  lines, with  $\varepsilon = 1$ .

The wavevector in tight-binding Hamiltonian (2) is measured from  $\Gamma$  point. Performing the rotation to the basis of  $C_4$  symmetry group defined in Eq.(23) via the

unitary matrix

$$U_{C_{4v}} = \begin{pmatrix} \frac{1}{2} & \frac{1}{\sqrt{2}} & 0 & \frac{1}{2} \\ \frac{1}{2} & 0 & \frac{1}{\sqrt{2}} & -\frac{1}{2} \\ \frac{1}{2} & -\frac{1}{\sqrt{2}} & 0 & \frac{1}{2} \\ \frac{1}{2} & 0 & -\frac{1}{\sqrt{2}} & -\frac{1}{2} \end{pmatrix}, \quad (\text{A2})$$

we find the transformed Hamiltonian:

---


$$U_{C_{4v}}^\dagger H U_{C_{4v}} = \frac{t_1}{2} \begin{pmatrix} -4\alpha - \cos(ak_x) - \cos(ak_y) & i\sqrt{2}\sin(ak_x) & i\sqrt{2}\sin(ak_y) & -\cos(ak_x) + \cos(ak_y) \\ -i\sqrt{2}\sin(ak_x) & 2\cos(ak_x) & 0 & -i\sqrt{2}\sin(ak_x) \\ -i\sqrt{2}\sin(ak_y) & 0 & 2\cos(ak_y) & i\sqrt{2}\sin(ak_y) \\ -\cos(ak_x) + \cos(ak_y) & i\sqrt{2}\sin(ak_x) & -i\sqrt{2}\sin(ak_y) & 4\alpha - \cos(ak_x) - \cos(ak_y) \end{pmatrix}. \quad (\text{A3})$$

---

It can be clearly seen that along flat line direction  $k_x a = 0$

---

(and similarly for  $k_y a = 0$ ), the Hamiltonian reduces to the block-diagonal matrix

---


$$U_{C_{4v}}^\dagger H U_{C_{4v}}(k_x = 0, k_y) = \frac{t_1}{2} \begin{pmatrix} -1 - 4\alpha - \cos(ak_y) & 0 & i\sqrt{2}\sin(ak_y) & -1 + \cos(ak_y) \\ 0 & 2 & 0 & 0 \\ -i\sqrt{2}\sin(ak_y) & 0 & 2\cos(ak_y) & i\sqrt{2}\sin(ak_y) \\ -1 + \cos(ak_y) & 0 & -i\sqrt{2}\sin(ak_y) & -1 + 4\alpha - \cos(ak_y) \end{pmatrix}. \quad (\text{A4})$$

Thus, one can conclude that the presence of flat lines is protected not only by  $C_4$  symmetry, but also by the geometry of tight-binding model. As was noted in Ref.[8], at the  $\Gamma$  point the flat lines represent nearly flat band (two lines intersect at the angle  $\frac{\pi}{2}$ ). When the two hopping parameters are equal,  $\alpha = 1$ , the corresponding linear low-energy model (24) treats the middle band as completely flat and is similar to a pseudospin-1 model. However, in the second order approximation (see Eq.(29)) the middle band becomes dispersive. This fact distinguishes this pseudospin-1 model from other models, such as Lieb [43], Kagome [44] or  $\alpha - T_3$  [37, 45, and 46] models, where the presence of exactly flat band is supported by the lattice geometry in tight-binding approximation.

---

## Appendix B: Green function of T-graphene and Hamiltonian derivatives

In this Appendix we calculate the Green function of the tight-binding Hamiltonian (2). Standardly it is defined as

$$G(\mathbf{k}, \varepsilon) = \frac{1}{t_1} \left( \varepsilon - \frac{1}{t_1} H(\mathbf{k}) \right)^{-1} \quad (\text{B1})$$

for energy  $\varepsilon$  measured in units of  $t_1$ . Using the formula for adjoint matrix, we find the simple but long expression. Decomposing it into blocks for the clarity of presentation, we write:

$$G(\mathbf{k}, \varepsilon) = \frac{1}{t_1 \det[\varepsilon - \frac{1}{t_1} H(\mathbf{k})]} \begin{pmatrix} G_{11} & G_{12} \\ G_{12}^\dagger & G_{22} \end{pmatrix}. \quad (\text{B2})$$

The corresponding blocks are given by the following expressions:

$$G_{11}(\mathbf{k}, \varepsilon) = \begin{pmatrix} \varepsilon(-2\alpha^2 + \varepsilon^2 - 1) + 2\alpha^2 \cos(k_y a) & \alpha e^{-ik_y a}(-\varepsilon + e^{ik_x a})(-1 + \varepsilon e^{ik_y a}) \\ \alpha e^{-ik_x a}(-1 + \varepsilon e^{ik_x a})(-\varepsilon + e^{ik_y a}) & \varepsilon(-2\alpha^2 + \varepsilon^2 - 1) + 2\alpha^2 \cos(k_x a) \end{pmatrix} \quad (\text{B3})$$

$$G_{12}(\mathbf{k}, \varepsilon) = \begin{pmatrix} 2\alpha^2(\varepsilon - \cos(k_y a)) - (\varepsilon^2 - 1)e^{ik_x a} & \alpha(-\varepsilon + e^{ik_x a})(\varepsilon - e^{ik_y a}) \\ \alpha(-\varepsilon + e^{ik_x a})(\varepsilon - e^{ik_y a}) & 2\alpha^2(\varepsilon - \cos(k_x a)) - (\varepsilon^2 - 1)e^{ik_y a} \end{pmatrix} \quad (\text{B4})$$

$$G_{22}(\mathbf{k}, \varepsilon) = \begin{pmatrix} \varepsilon(-2\alpha^2 + \varepsilon^2 - 1) + 2\alpha^2 \cos(k_y a) & \alpha e^{-ik_x a}(-1 + \varepsilon e^{ik_x a})(-\varepsilon + e^{ik_y a}) \\ \alpha e^{-ik_y a}(-\varepsilon + e^{ik_x a})(-1 + \varepsilon e^{ik_y a}) & \varepsilon(-2\alpha^2 + \varepsilon^2 - 1) + 2\alpha^2 \cos(k_x a) \end{pmatrix}. \quad (\text{B5})$$

These expressions are used to evaluate the (37) and (38) traces in the main text.

- 
- <sup>1</sup> Yu Liu, Gang Wang, Qingsong Huang, Liwei Guo, and Xiaolong Chen, “Structural and Electronic Properties of *T* Graphene: A Two-Dimensional Carbon Allotrope with Tetrarings,” *Physical Review Letters* **108**, 225505 (2012).
- <sup>2</sup> H. Terrones, M. Terrones, E. Hernández, N. Grobert, J.-C. Charlier, and P. M. Ajayan, “New metallic allotropes of planar and tubular carbon,” *Phys. Rev. Lett.* **84**, 1716–1719 (2000).
- <sup>3</sup> Andrey N. Enyashin and Alexander L. Ivanovskii, “Graphene allotropes,” *Physica Status Solidi (b)* **248**, 1879–1883 (2011).
- <sup>4</sup> Bog G. Kim, Jun Young Jo, and H. S. Sim, “Comment on “Structural and Electronic Properties of *T* Graphene: A Two-Dimensional Carbon Allotrope with Tetrarings”,,” *Phys. Rev. Lett.* **110**, 029601 (2013).
- <sup>5</sup> Jian Sun Qinyan Gu, Dingyu Xing, “Superconducting single-layer T-graphene and novel synthesis routes,” *Chinese Physics Letters* **36**, 097401 (2019).
- <sup>6</sup> Xian-Lei Sheng, Hui-Juan Cui, Fei Ye, Qing-Bo Yan, Qing-Rong Zheng, and Gang Su, “Octagraphene as a versatile carbon atomic sheet for novel nanotubes, unconventional fullerenes, and hydrogen storage,” *Journal of Applied Physics* **112**, 074315 (2012).
- <sup>7</sup> An Bao, Hong-Shuai Tao, Hai-Di Liu, XiaoZhong Zhang, and Wu-Ming Liu, “Quantum magnetic phase transition in square-octagon lattice,” *Scientific Reports* **4**, 6918 (2014).
- <sup>8</sup> Yasufumi Yamashita, Masaki Tomura, Yuki Yanagi, and Kazuo Ueda, “SU(3) Dirac electrons in the  $\frac{1}{5}$ -depleted square-lattice Hubbard model at  $\frac{1}{4}$  filling,” *Physical Review B* **88**, 195104 (2013).
- <sup>9</sup> Weifeng Li, Meng Guo, Gang Zhang, and Yong-Wei Zhang, “Gapless MoS<sub>2</sub> allotrope possessing both massless Dirac and heavy fermions,” *Phys. Rev. B* **89**, 205402 (2014).
- <sup>10</sup> Nicholas Pomata and Tzu-Chieh Wei, “Demonstrating the AKLT spectral gap on 2D degree-3 lattices,” arxiv:1911.01410 (2019), 1911.01410v2.
- <sup>11</sup> Yan Sun, Claudia Felser, and Binghai Yan, “Graphene-like Dirac states and quantum spin Hall insulators in square-octagonal *MX*<sub>2</sub> (*M* = Mo, W; *X* = S, Se, Te) isomers,” *Physical Review B* **92**, 165421 (2015).
- <sup>12</sup> Koichiro Umemoto, Renata M. Wentzcovitch, Susumu Saito, and Takashi Miyake, “Body-Centered Tetragonal C<sub>4</sub>: A Viable *sp*<sup>3</sup> Carbon Allotrope,” *Physical Review Letters* **104**, 125504 (2010).
- <sup>13</sup> R. Majidi, “Electronic properties of T graphene-like C–BN sheets: A density functional theory study,” *Phys. E: Low-dim. Sys. and Nanostr.* **74**, 371–376 (2015).
- <sup>14</sup> R. Majidi, “Density functional theory study on structural and mechanical properties of graphene, T-graphene, and R-graphyne,” *Theoretical Chemistry Accounts* **136**, 109 (2017).
- <sup>15</sup> Wen-Jin Yin, Yue-E. Xie, Li-Min Liu, Ru-Zhi Wang, Xiao-Lin Wei, Leo Lau, Jian-Xin Zhong, and Yuan-Ping Chen, “R-graphyne: a new two-dimensional carbon allotrope with versatile Dirac-like point in nanoribbons,” *Journal of Materials Chemistry A* **1**, 5341 (2013).
- <sup>16</sup> A. I. Podlivaev and L. A. Openov, “Kinetic stability of octagraphene,” *Physics of the Solid State* **55**, 2592–2595 (2013).
- <sup>17</sup> Prashant Vijay Gaikwad and Anjali Kshirsagar, “Octagonal family of monolayers, bulk and nanotubes,” arxiv:2003.00158 (2020), <http://arxiv.org/abs/2003.00158v1>.
- <sup>18</sup> Noah F. Q. Yuan, Hiroki Isobe, and Liang Fu, “Magic of high-order van Hove singularity,” *Nature Communications* **10**, 5769 (2019).
- <sup>19</sup> G. Vignale, “Orbital paramagnetism of electrons in a two-dimensional lattice,” *Physical Review Letters* **67**, 358–361 (1991).
- <sup>20</sup> Rahul Nandkishore, L. S. Levitov, and A. V. Chubukov, “Chiral superconductivity from repulsive interactions in doped graphene,” *Nature Physics* **8**, 158–163 (2012).
- <sup>21</sup> Hiroki Isobe and Liang Fu, “Supermetal,” *Physical Review Research* **1**, 033206 (2019).
- <sup>22</sup> Barry Bradlyn, Jennifer Cano, Zhijun Wang, M. G. Vergniory, C. Felser, R. J. Cava, and B. Andrei Bernevig, “Beyond Dirac and Weyl fermions: Unconventional quasiparticles in conventional crystals,” *Science* **353**, aaf5037 (2016).
- <sup>23</sup> A. Shtyk, G. Goldstein, and C. Chamon, “Electrons at the monkey saddle: A multicritical Lifshitz point,” *Physical Review B* **95**, 035137 (2017).
- <sup>24</sup> Dmitry V. Efremov, Alex Shtyk, Andreas W. Rost, Claudio Chamon, Andrew P. Mackenzie, and Joseph J. Betouras, “Multicritical Fermi Surface Topological Transitions,” *Physical Review Letters* **123**, 207202 (2019).
- <sup>25</sup> Aline Ramires, Piers Coleman, Andriy H. Nevidomskyy,

- and A. M. Tsvelik, “ $\beta$ -YbAlB<sub>4</sub>: A critical nodal metal,” *Physical Review Letters* **109**, 176404 (2012).
- <sup>26</sup> Laura Classen, Andrey V. Chubukov, Carsten Honerkamp, and Michael M. Scherer, “Competing orders at higher-order Van Hove points,” [2006.14729v1](#).
  - <sup>27</sup> Yu-Ping Lin and Rahul M. Nandkishore, “Parquet renormalization group analysis of weak-coupling instabilities with multiple high-order Van Hove points inside the Brillouin zone,” [2008.05485v1](#).
  - <sup>28</sup> N. W. Ashcroft and N. D. Mermin, *Solid State Physics* (Saunders College Publishing, Fort Worth., 1976).
  - <sup>29</sup> G. Gómez-Santos and T. Stauber, “Measurable lattice effects on the charge and magnetic response in graphene,” *Phys. Rev. Lett.* **106**, 045504 (2011).
  - <sup>30</sup> Arnaud Raoux, Frédéric Piéchon, Jean-Noël Fuchs, and Gilles Montambaux, “Orbital magnetism in coupled-bands models,” *Phys. Rev. B* **91**, 085120 (2015).
  - <sup>31</sup> Jun Li, Shangjian Jin, Fan Yang, and Dao-Xin Yao, “Electronic structure, magnetism and high-temperature superconductivity in the multi-layer octagraphene and octagraphite,” [2008.09620v1](#).
  - <sup>32</sup> Thibaud Louvet, Pierre Delplace, Andrei A. Fedorenko, and David Carpentier, “On the origin of minimal conductivity at a band crossing,” *Physical Review B* **92**, 155116 (2015).
  - <sup>33</sup> Per-Olov Löwdin, “A note on the quantum-mechanical perturbation theory,” *The Journal of Chemical Physics* **19**, 1396–1401 (1951).
  - <sup>34</sup> Lih-King Lim, Jean-Noël Fuchs, Frédéric Piéchon, and Gilles Montambaux, “Dirac points emerging from flat bands in Lieb-kagome lattices,” *Phys. Rev. B* **101**, 045131 (2020).
  - <sup>35</sup> Frédéric Piéchon, Arnaud Raoux, Jean-Noël Fuchs, and Gilles Montambaux, “Geometric orbital susceptibility: Quantum metric without Berry curvature,” *Phys. Rev. B* **94**, 134423 (2016).
  - <sup>36</sup> Hidetoshi Fukuyama, “Theory of orbital magnetism of Bloch electrons: Coulomb interactions,” *Progress of Theoretical Physics* **45**, 704–729 (1971).
  - <sup>37</sup> A. Raoux, M. Morigi, J.-N. Fuchs, F. Piéchon, and G. Montambaux, “From dia- to paramagnetic orbital susceptibility of massless fermions,” *Physical Review Letters* **112**, 026402 (2014).
  - <sup>38</sup> L. Landau, “Diamagnetismus der metalle,” *Zeitschrift für Physik* **64**, 629–637 (1930).
  - <sup>39</sup> R. Peierls, “Zur theorie des diamagnetismus von leitungselektronen,” *Zeitschrift für Physik* **80**, 763–791 (1933).
  - <sup>40</sup> L. D. Landau and E. M. Lifshitz, *Course of Theoretical Physics*, Vol. 9, Pt. 2, Sec.57. (Pergamon, New York., 1981).
  - <sup>41</sup> J. W. McClure, “Diamagnetism of graphite,” *Physical Review* **104**, 666–671 (1956).
  - <sup>42</sup> Philipp Rosenzweig, Hrag Karakachian, Dmitry Marchenko, Kathrin Kster, and Ulrich Starke, “Overdoping graphene beyond the van Hove singularity,” [2009.04876](#).
  - <sup>43</sup> R. Shen, L. B. Shao, Baigeng Wang, and D. Y. Xing, “Single Dirac cone with a flat band touching on line-centered-square optical lattices,” *Phys. Rev. B* **81**, 041410 (2010).
  - <sup>44</sup> Dmitry Green, Luiz Santos, and Claudio Chamon, “Isolated flat bands and spin-1 conical bands in two-dimensional lattices,” *Phys. Rev. B* **82**, 075104 (2010).
  - <sup>45</sup> E. V. Gorbar, V. P. Gusynin, and D. O. Oriekhov, “Electron states for gapped pseudospin-1 fermions in the field of a charged impurity,” *Physical Review B* **99**, 155124 (2019).
  - <sup>46</sup> D. O. Oriekhov, E. V. Gorbar, and V. P. Gusynin, “Electronic states of pseudospin-1 fermions in dice lattice ribbon,” *Low Temperature Physics* **44**, 1313–1324 (2018).